Figure S1. The time series of relative humidity profiles (units: %) from ARM interpolated soundings at the Azores (39.09°N, -28.02°W) on (a) 1 July 2016, (c) 19 July 2017, and (e) 23 August 2019. Panels (b), (d), and (f) depict the same dates as (a), (c), and (e), respectively, but show the average relative humidity from WRF-Chem simulated data over a 20 × 20 grid centered on the Azores (approximately 4 km resolution).
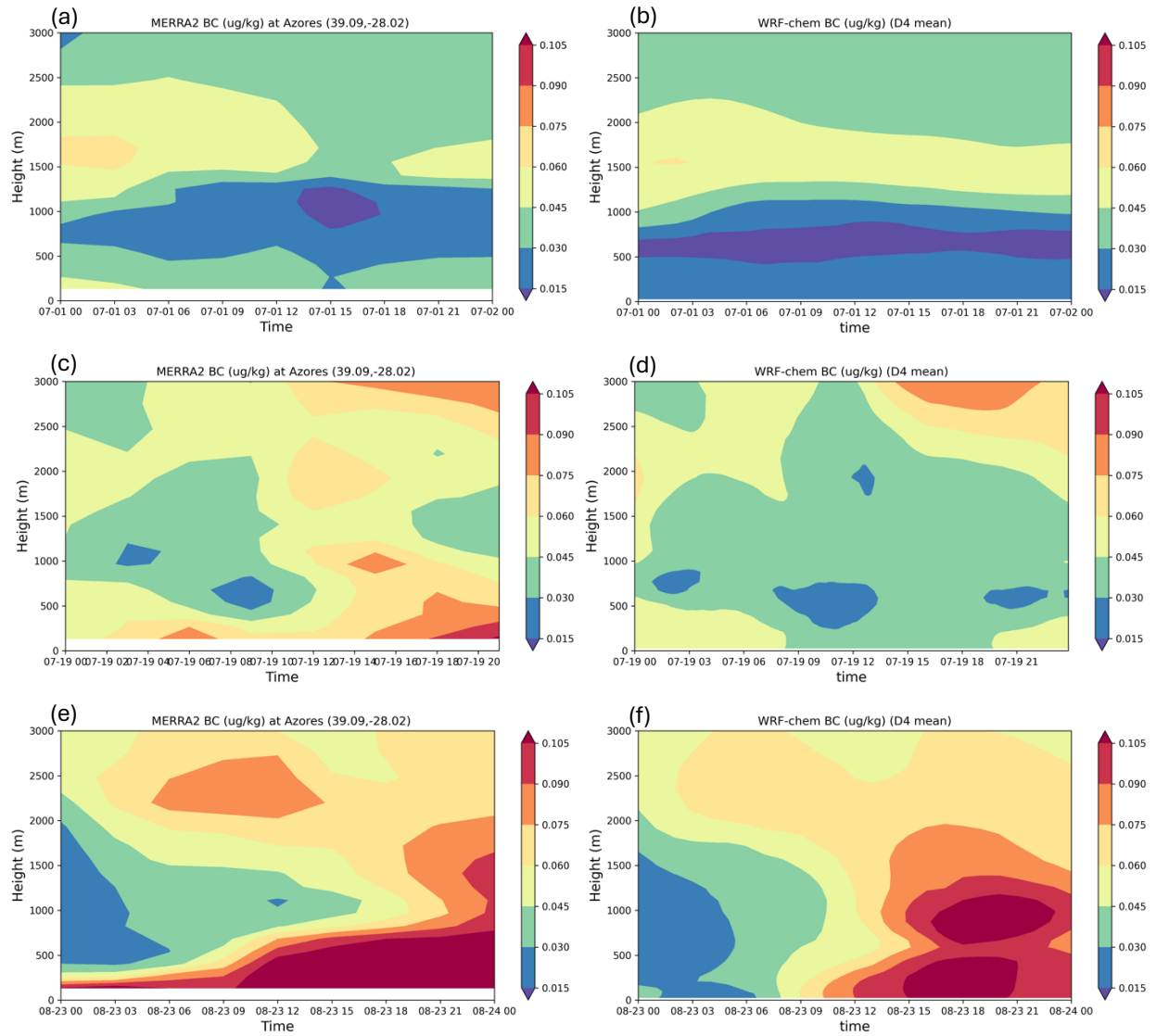
Figure S2. The time series of BC profiles (units: µg kg^{-1}) from MERRA-2 at the Azores (39.09°N, -28.02°W) on (a) 1 July 2016, (c) 19 July 2017, and (e) 23 August 2019. Panels (b), (d), and (f) depict the same dates as (a), (c), and (e), respectively, but show the average aerosol concentration from WRF-Chem simulated data over the domain 4.
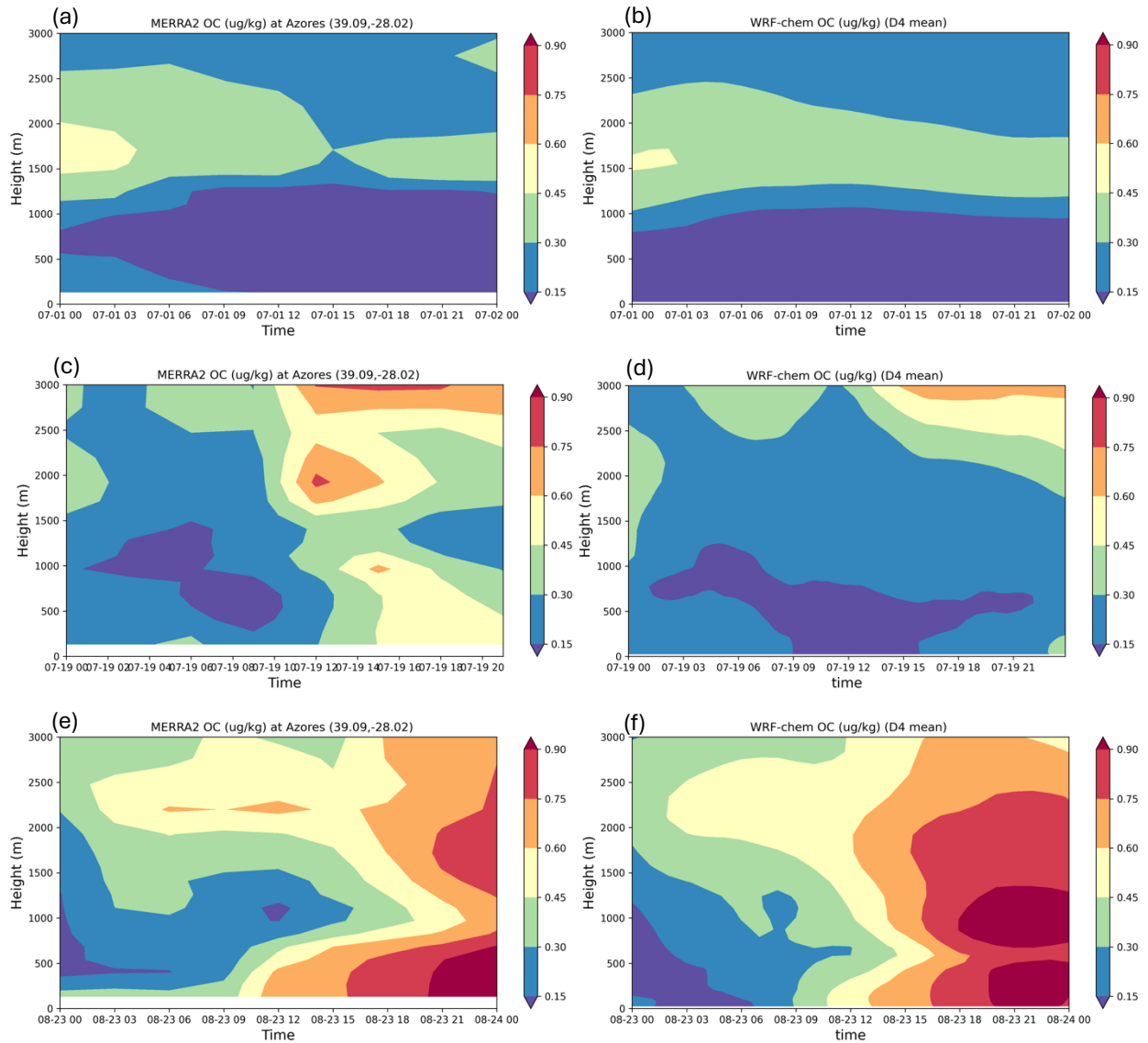
Figure S3. The time series of OC profiles (units: μg kg^{-1}) from MERRA-2 at the Azores (39.09°N, -28.02°W) on (a) 1 July 2016, (c) 19 July 2017, and (e) 23 August 2019. Panels (b), (d), and (f) depict the same dates as (a), (c), and (e), respectively, but show the average aerosol concentration from WRF-Chem simulated data over the domain 4.
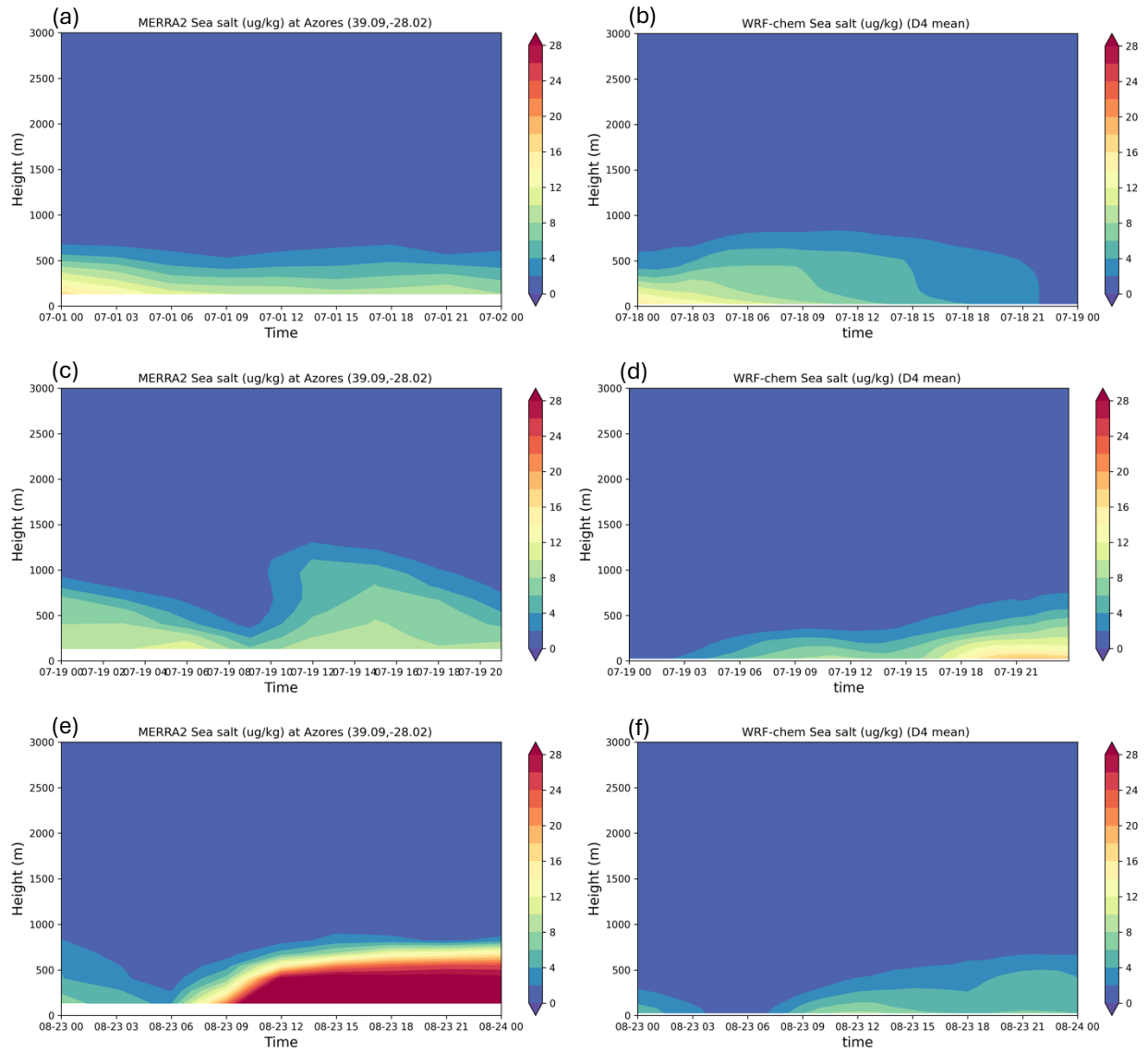
Figure S4. The time series of sea salt profiles (units: µg kg^{-1}) from MERRA-2 at the Azores (39.09°N, -28.02°W) on (a) 1 July 2016, (c) 19 July 2017, and (e) 23 August 2019. Panels (b), (d), and (f) depict the same dates as (a), (c), and (e), respectively, but show the average aerosol concentration from WRF-Chem simulated data over the domain 4.
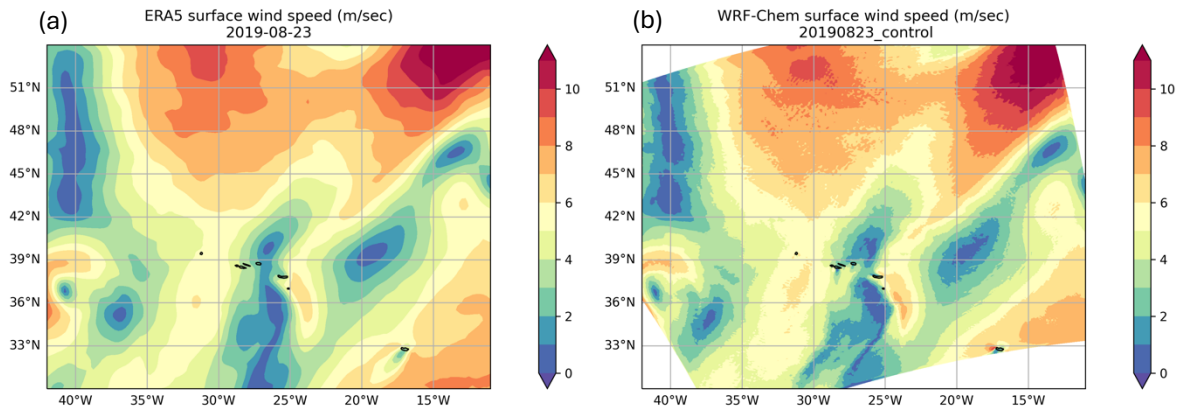
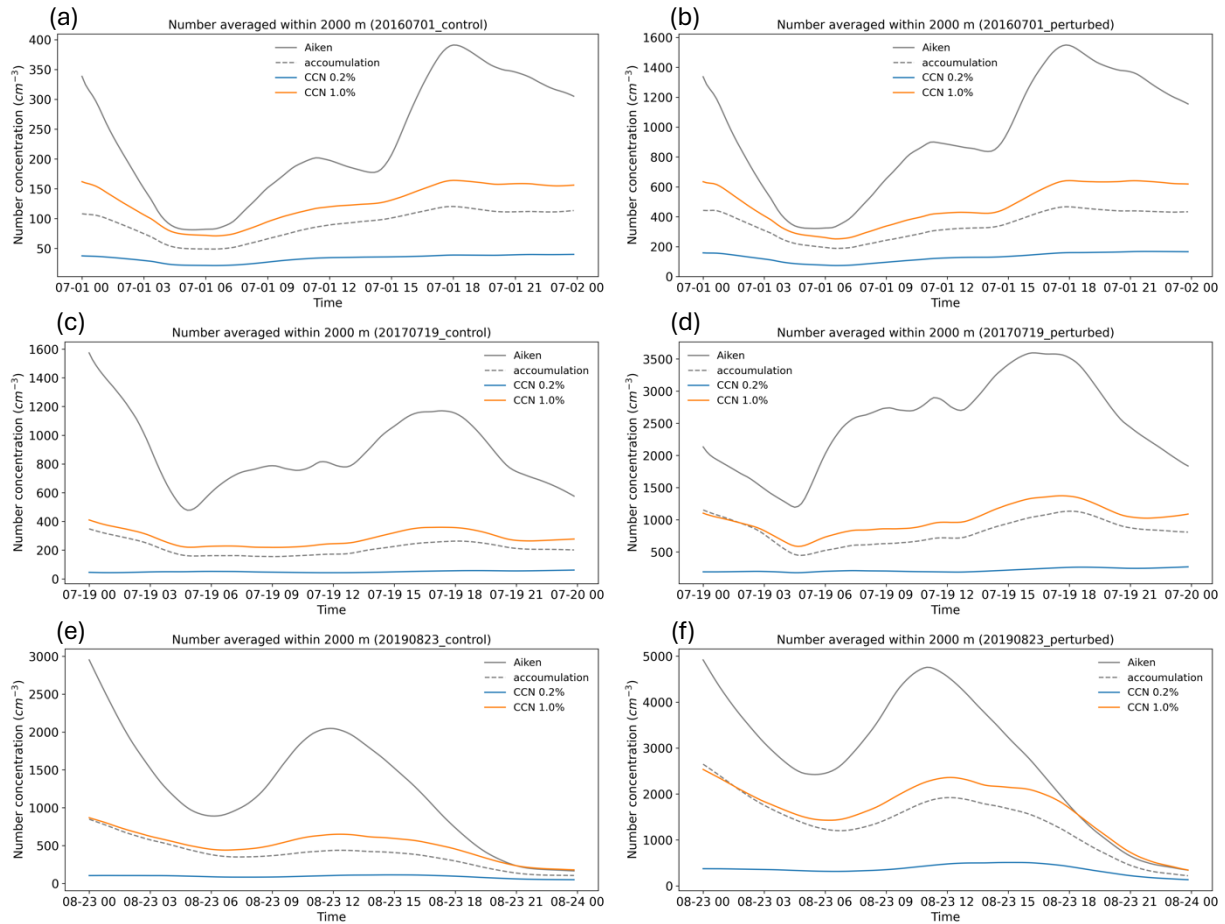Figure S5. (a) ERA5 and (b) WRF-Chem (d01) mean surface wind speed (contour; units: m sec^{-1}) on 23 August 2019.

Figure S6. (a), (c), and (e) are the time series of domain-averaged aerosol number concentration (Aiken mode and accumulation mode; units: cm^{-3}) and CCN number concentration under 0.2% and 1.0% supersaturations (units: cm^{-3} averaged within 2000 m height over the domain 4 on 1 July 2016, 19 July 2017, and 23 August 2019, respectively, in the control runs. (b), (d), and (f) are the same as (a), (c), and (e) but in the perturbed runs.
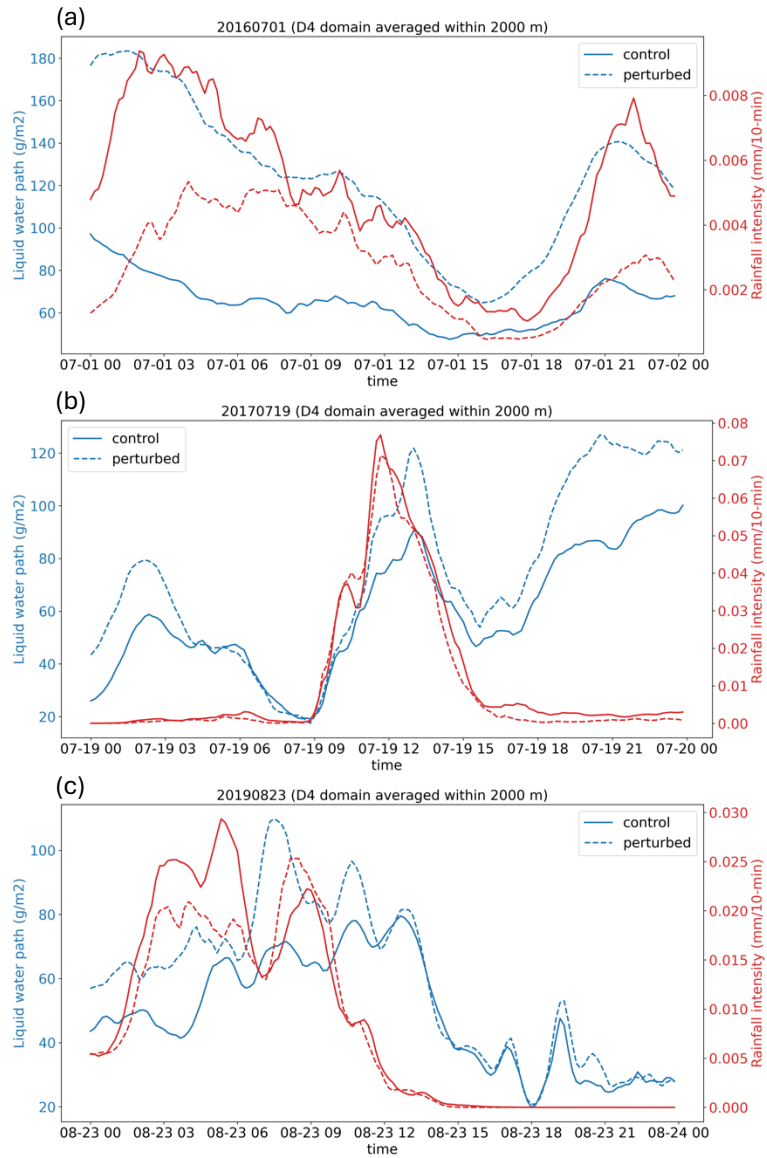
Figure S7. (a), (b), and (c) are he time series of domain-averaged liquid water path (blue lines; units: g m⁻²) and rainfall intensity (red lines; units: mm 10-min⁻¹) for the control case (soild lines) and the perturbed case (dashed lines) on 1 July 2016, 19 July 2017, and 23 August 2019, respectively.
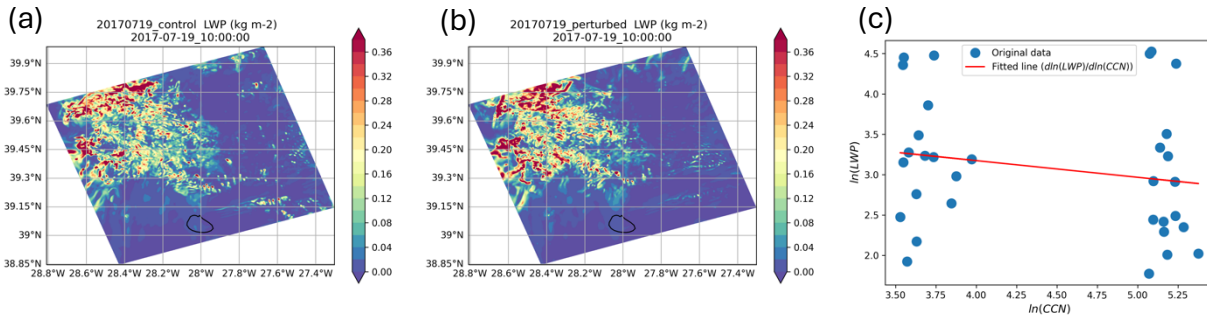
Figure S8. WRF-Chem simulated liquid water path (LWP; units: kg m^{-2}) in (a) the control run and (b) the perturbed runs at 10:00 UTC on 19 July 2017 over the domain 4. (c) The logarithmic slope between LWP and CCN using data from 16 aggregate grid points (~25 km for each grid point) from (a) the control run and 16 aggregated grid points from (b) the perturbed run.
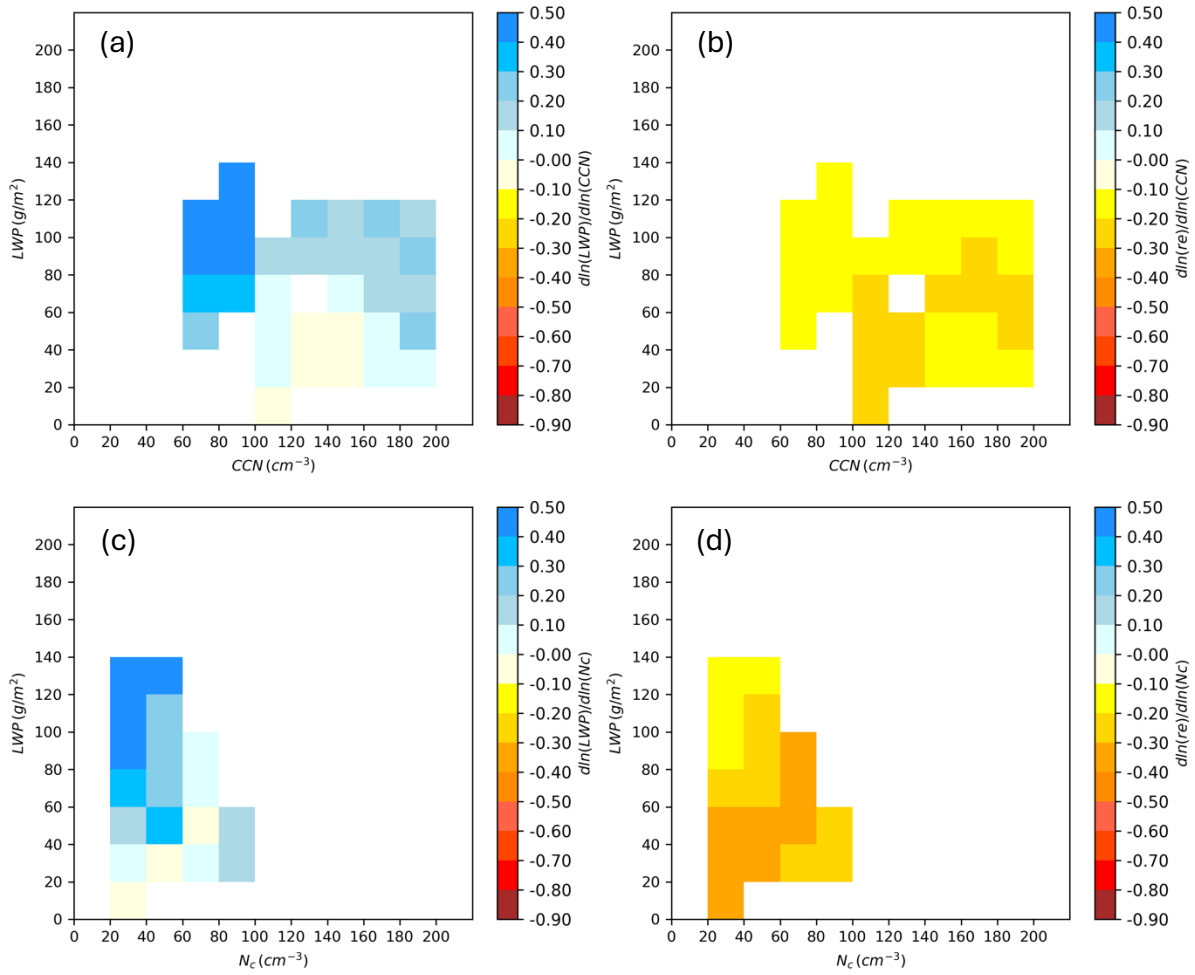
Figure S9. (a) and (b) are the mean liquid water path (LWP) and cloud radius (Re) susceptibilities for different cloud condensation nuclei (CCN) and LWP bins for three study cases, respectively. (c) and (d) are the same as (a) and (b), respectively, but for different cloud droplet number (Nc) and LWP bins.
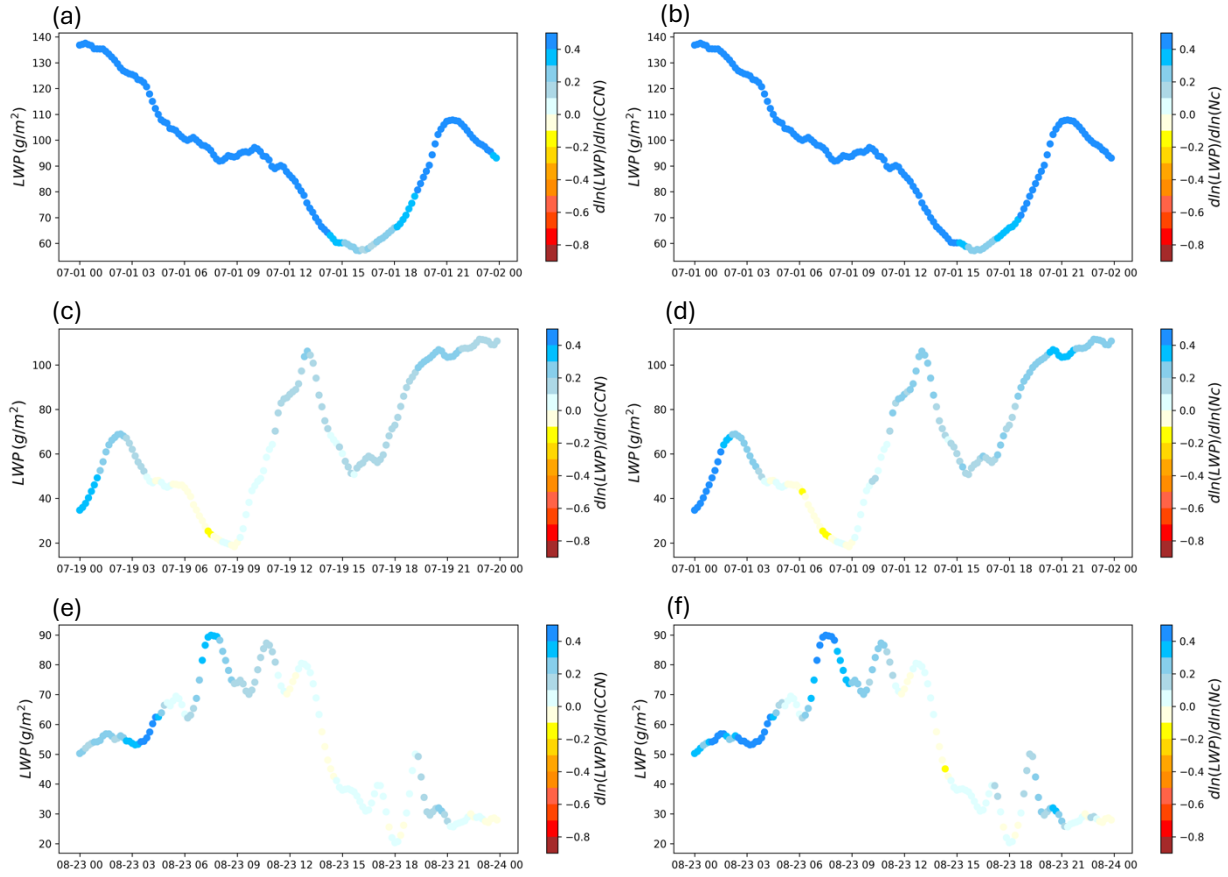
Figure S10. (a), (c) and (e) are the time variable of LWP susceptibility for different CCN concentration on 1 July 2016, 19 July 2017, and 23 August 2019, respectively. (b), (d) and (f) are the time variable of LWP susceptibility for different Nc concentration on 1 July 2016, 19 July 2017, and 23 August 2019, respectively.